AIAA AVIATION Forum
5-9 June 2017, Denver, Colorado
17th AIAA Aviation Technology, Integration, and Operations Conference

An Alternative Time Metric to Modified Tau for Unmanned Aircraft System Detect And Avoid

Minghong G. Wu *
NASA Ames Research Center Moffett Field CA 94035, USA

Vibhor L. Bageshwar † and Eric A. Euteneuer ‡
Advanced Technology, Honeywell Aerospace,
Honeywell International, Golden Valley, MN 55422, USA

A new horizontal time metric, Time to Protected Zone, is proposed for use in the Detect and Avoid (DAA) Systems equipped by unmanned aircraft systems (UAS). This time metric has three advantages over the currently adopted time metric, modified tau: it corresponds to a physical event, it is linear with time, and it can be directly used to prioritize intruding aircraft. The protected zone defines an area around the UAS that can be a function of each intruding aircraft's surveillance measurement errors. Even with its advantages, the Time to Protected Zone depends explicitly on encounter geometry and may be more sensitive to surveillance sensor errors than modified tau. To quantify its sensitivity, simulation of 972 encounters using realistic sensor models and a proprietary fusion tracker is performed. Two sensitivity metrics, the probability of time reversal and the average absolute time error, are computed for both the Time to Protected Zone and modified tau. Results show that the sensitivity of the Time to Protected Zone is comparable to that of modified tau if the dimensions of the protected zone are adequately defined.

Nomenclature

D_{mod}	incremental distance modifier
HMD	horizontal miss distance
P_r	probability of time reversal
R_0	radius of disk inside a protected zone
R_c	characteristic range for alerting
h	altitude difference
$\dot{\mathbf{r}}$	relative (horizontal) velocity vector
$\mathbf{r}$	relative (horizontal) position vector
r	range
$\dot{r}$	range rate
t_{cpa}	time to the horizontal closest point of approach
t_{pz}	time to Protected Zone
v	relative speed, magnitude of the $\dot{\mathbf{r}}$ vector
v_c	characteristic relative speed
x	horizontal coordinate on the collision plane
y	vertical coordinate on the collision plane
τ_{mod}	modified tau
$\lvert\Delta\rvert_{avg}$	average absolute error of a time metric
Δ_H	characteristic size of the additional buffer zone

*Research Engineer, Aviation Systems, AIAA member
†Principal Scientist
‡Technology Portfolio Manager

$\Delta_H{}^0$	benchmark Δ_H
σ_H	standard deviation of HMD as a result of surveillance errors
σ_b	standard deviation of bearing measurement
σ_p	standard deviation of position measurement
σ_r	standard deviation of range measurement
$\sigma_{\dot{r}}$	standard deviation of range rate measurement
σ_v	standard deviation of speed measurement
$(\ )^*$	threshold

I. Introduction

Successful development and validation of performance standards for Detect and Avoid (DAA) Systems serve as a crucial step for the integration of Unmanned Aircraft System (UAS) operations in the National Airspace System (NAS). A DAA system provides alerts and guidance to keep a UAS "Well Clear" of other aircraft.[1,2] In the United States, a significant number of simulation tests as well as flight tests have been conducted to provide supporting information for selecting an adequate definition of DAA Well Clear[1,3] and requirements for the alerting performance.[4–7] Prototype DAA alerting and guidance algorithms have also been developed.[8–10] The RTCA Special Committee 228 (SC-228) Working Group I recently finished its Phase I work at the end of 2016, and it is in the process of publishing the Minimum Operational Performance Standards (MOPS) for DAA systems. This Phase I MOPS targets UAS capable of carrying large and high-power sensor systems for operations in non-terminal areas. UAS in this category will be equipped with surveillance systems including Automatic Dependent Surveillance-Broadcast (ADS-B) in, airborne active surveillance, an air-to-air radar, as well as a DAA tracker that processes surveillance data. Phase II work for extending the MOPS to additional UAS categories and operations is underway.

The DAA Well Clear (DWC) zone for the UAS targeted in the Phase I MOPS is defined by thresholds of three parameters. It does not have distinct physical boundaries because the definition depends on two aircraft's relative position and velocity during an encounter. Figure 1 illustrates a DWC zone. The Horizontal Miss Distance (HMD) represents the two aircraft's predicted minimum horizontal distance during an encounter assuming constant velocities (see Appendix A for a mathematical definition). The parameter h represents the two aircraft's current altitude difference. The time metric modified tau, τ_{mod}, is an estimated time taken for the two aircraft to get horizontally close to each other (to be discussed in great detail below). The thresholds, denoted by an asterisk, for the HMD, h, and τ_{mod} are 4000 ft, 450 ft, and 35 sec, respectively. All three parameters must simultaneously fall below their respective thresholds during an encounter for the two aircraft to violate the DWC. Alerting algorithms are designed to reduce the probability of violating DWC to a value required by the MOPS. The MOPS describes alerting requirements in terms of probabilities and test vectors without dictating a specific alerting algorithm. Prior research to inform the MOPS defined raw alerts using the same definitions as the DWC but with larger thresholds to provide buffers for surveillance uncertainties.[5]

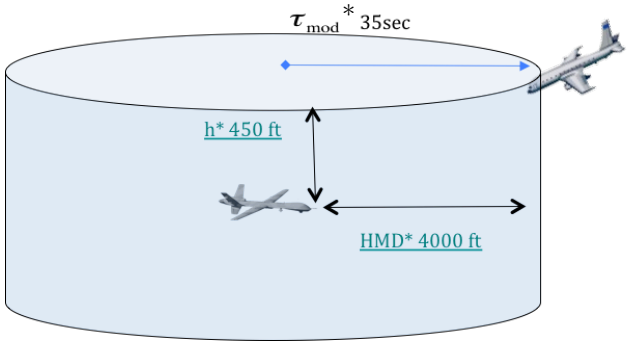

Figure 1. A schematic representation of the DWC zone.

The definition of τ_{mod} is[2]

$$\tau_{mod} = \begin{cases} -\frac{r^2 - {D_{\text{mod}}}^2}{r\dot{r}}, r > D_{\text{mod}}, \\ 0, r \leq D_{\text{mod}} \end{cases} \quad (1)$$

where r and $\dot{r}$ are the horizontal range and range rate between the intruding aircraft (referred to as the intruder) and the UAS (referred to as the ownship), respectively. The range rate is negative for closing geometries. The positive incremental distance modifier D_{mod} defines the radius of a "protection" disk around the ownship such that any intruder with a horizontal range less than D_{mod} is always considered "urgent". In this case, $\tau_{mod} = 0$.

The time metric τ_{mod}, however, has certain limiting properties:

- It does not correspond to the time of any physical event.
- It is nonlinear with time, especially in the vicinity of the D_{mod} disk (see Section III for an example).
- During a multi-intruder encounter, τ_{mod} cannot be directly used to prioritize intruders.

The time metric τ_{mod} has been used by the Traffic Alert and Collision Avoidance System (TCAS) II equipped by many manned aircraft.[11] TCAS II is an optional component for the UAS targeted in Phase I MOPS. Nonetheless, interoperability between a DAA system and TCAS II has been a driving force in defining the Phase I MOPS. Ideally, a DWC zone should enclose TCAS's alerting zone for its resolution advisory. Because of this consideration, one argument for using τ_{mod} for the DAA DWC is for potential better interoperability with TCAS II. The choice of τ_{mod}, however, turns out to have minimal effects due to additional differences in TCAS II and DAA's alerting logic such as the following:

1. TCAS II does not use the HMD consistently in its alerting logic; and
2. TCAS II's τ_{mod} is based on 3-D range and range rates whereas the τ_{mod} defined for a DAA system is based on horizontal range and range rate.

Another argument for using τ_{mod} for DAA systems is that the range-based τ_{mod} avoids bearing measurements and its large measurement error. The bearing measurement errors are large in the active surveillance used by TCAS and, therefore, τ_{mod} is a good choice for TCAS. However, for the DAA system, The bearing measurement error is much less of an issue since the DAA system considered by the MOPS will use ADS-B and an air-to-air radar, which both provide ten times more accurate bearing measurements than the active surveillance used by TCAS.

This paper proposes a new, alternative horizontal time metric, the Time to Protected Zone, denoted by t_{pz}. This metric has three advantages over τ_{mod}: it corresponds to a physical event, it is linear with time, and it can be used directly in prioritizing intruders during a multi-intruder encounter. For alerting purposes, the protected zone is extended to be a function of surveillance sensor measurement errors, or surveillance errors. Since the time metric t_{pz} utilizes bearing measurements and, therefore, it may be too sensitive to bearing measurement errors to be effective for alerting. To quantify sensitivities to surveillance errors, simulations of 972 encounters are conducted using two sensitivity metrics to compare τ_{mod} and t_{pz}. The parameters of the encounters are organized into an encounter test matrix. The surveillance sensor errors are modeled by Honeywell's sensor models and proprietary sensor fusion tracker.[12]

The paper is organized as follows. Section II supplies additional background information and describes the definition of t_{pz}. Section III discusses issues about using τ_{mod} that can be overcome by t_{pz}. Section IV defines the sensitivity criteria for the time metrics. Section V describes the encounter test matrix and the simulation setup. Section VI presents results and discussions. Section VII concludes the paper.

II. Time to Protected Zone

II.A. Background

The development of the MOPS for DAA systems uses a time metric to evaluate the horizontal separation between two aircraft. A fast-approaching intruder 8 nmi away may pose a more urgent threat than a slow-approaching intruder 3 nmi away. With a time metric threshold, the DWC does not have a fixed, physical volume; rather it is a function of the intruder's relative horizontal position and velocity. The time window

considered by a DAA system covers up to 3 minutes before the aircraft reach their minimum horizontal separation.

A commonly used time metric for pilots' situation awareness and intruder prioritization is the time to the Closest Point of Approach (CPA), denoted as t_{cpa}. This time metric corresponds to a physical event and it is linear with time. However, t_{cpa} underestimates the urgency of an encounter when the intruder and ownship are flying almost parallel trajectories at close range. The metric τ_{mod} mitigates this problem by introducing a disk around the ownship with a radius of D_{mod}. Any intruder within the D_{mod} disk results in zero τ_{mod} and it is always considered an urgent threat. However, τ_{mod} does not correspond to any physical event. Also, τ_{mod} is non-linear with time, especially near the D_{mod} disk. With such behaviors, τ_{mod} cannot be used to prioritize intruders by any criteria (See Section III).

A time metric called the Time to Entry Point has been proposed as the predicted time for the intruder to reach the D_{mod} disk.[13,14] Any intruder inside the D_{mod} disk has a zero Time to Entry Point. This time metric maintains the advantages of both t_{cpa} and τ_{mod} and avoids their disadvantages. The Time to Entry Point is left undefined if the intruder is not predicted to enter the D_{mod} disk, i.e., its HMD is greater than D_{mod}.

II.B. Definition

This work proposes the Time to Protected Zone, t_{pz}, which extends the Time to Entry Point metric in the following aspects:

- The metric t_{pz} is defined as the time to reach a protected around the ownship that does not necessarily take the shape of a disk.
- When used for evaluating alerts, the dimensions of the protected zone can be made a function of the surveillance errors of each intruder.
- The metric t_{pz} is set to t_{cpa} when the intruder is not predicted to enter the protected zone. This provides an alerting algorithm with a continuous definition of time metric when the projected intruder trajectory moves in and out of the protected zone in real time.

Figure 2 demonstrates the definition of the protected zone at any time during an encounter. Consider a relative horizontal reference frame with two aircraft flying in a closing geometry. Without loss of generality, the ownship is placed at the origin of this reference frame. The axes, $\hat{x}$ and $\hat{y}$, are chosen such that the intruder's horizontal velocity vector relative to the ownship, $\dot{\mathbf{r}}$, points along the negative direction of the $\hat{y}$ axis. The intruder's relative horizontal position vector from the ownship is denoted by $\mathbf{r}$. This convention of axes is called the collision plane.[15,16] The ownship's true ground heading is not used for choosing the direction of the axes. In this reference frame, the intruder's distance from the $\hat{y}$ axis is always equal to the HMD.

There is flexibility in the choice of the shape and dimensions of the protected zone. Its dimensions can be made to depend on individual intruders' surveillance errors for improved alerting performance. The example protected zone in Figure 2 consists of a disk with radius R_0 and an additional buffer zone shown in blue. The boundary of the protected zone is shown in bold. For brevity, only the right-half plane enclosing the intruder is shown in Figure 2 as the protected zone is symmetric about the $\hat{y}$ axis. The additional buffer zone in blue is meant to accommodate HMD errors arising from surveillance errors.

The metric t_{pz} is defined as the time to reach the protected zone, or the time to reach the bold curve shown in Figure 2. If the intruder's HMD projects outside the protected zone, t_{pz} is defined to be the time to reach the horizontal $\hat{x}$ axis, i.e., $t_{pz} = t_{cpa}$ outside the protected zone. This definition ensures a smooth change of t_{pz} upon change of an intruder's HMD.

With this definition of a protected zone, it follows naturally that, when defining alert criteria, the HMD threshold, denoted as HMD*, should be consistently set to the edge of the protected zone.

Let the surface of the protected zone be described by $y = f(x)$. The function y is chosen such that it is symmetric with respect to x, i.e., $f(x) = f(-x)$, where $f(x) \geq 0$. Without loss of generality, consider a case in which the $\hat{x}$ component of the intruder's $\mathbf{r}$ is positive. By definition of the reference frame, x = HMD. Therefore, an intruder will be predicted to reach the protected zone at (HMD, y). Since y is the intersection of the the intruder's predicted trajectory with the protected zone, it is also the distance the intruder must

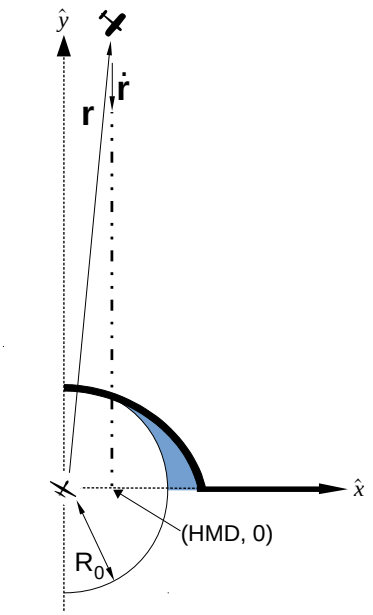

Figure 2. An example protected zone consisting of a disk with a radius R_0 and an additional buffer zone colored in blue.

fly to reach the CPA. Therefore,

$$t_{pz} = \max\left(0,\ t_{cpa} - \frac{y}{|\dot{\mathbf{r}}|}\right). \tag{2}$$

Note that $t_{cpa} - \frac{y}{|\dot{\mathbf{r}}|} < 0$ if the intruder is already within the protected zone.

The time metric t_{cpa} can be viewed as a special case of t_{pz}, for which the protected zone is defined to have zero area, i.e., $y = 0$ for every x.

II.C. Dimensions of the Protected Zone

In this paper, the surface, or boundary, of the protected zone is defined with the following function:

$$x = \sqrt{{R_0}^2 - y^2} + \left(1 - \frac{y}{R_0}\right)\Delta_H, \qquad 0 < y \le R_0 \text{ and } |x| \le R_0 + \Delta_H \tag{3a}$$

$$0 = y, \qquad |x| > R_0 + \Delta_H \tag{3b}$$

With this choice, the protected zone includes a R_0 disk and an additional buffer outside the disk that increases linearly as y approaches the $\hat{x}$ axis, reaching Δ_H at $y = 0$. This parameter Δ_H is user-selected and controls the size of the additional buffer zone. Solving for y in terms of x,

$$y = \begin{cases} \frac{1}{1+\left(\frac{\Delta_H}{R_0}\right)^2}\left[-\frac{\Delta_H}{R_0}(x-\Delta_H)^2 + \sqrt{-(x-\Delta_H)^2 + {R_0}^2 + {\Delta_H}^2}\right], & \text{when } |x| \le R_0 + \Delta_H, \\ 0 & \text{, when } x > R_0 + \Delta_H \end{cases} \tag{4}$$

II.D. Comparison of Time Metrics

All three time metrics described above, τ_{mod}, t_{pz}, and t_{cpa}, are symmetric,[17] meaning their values are preserved upon switching the ownship and the intruder's states. Table 1 compares and contrasts the properties of the three time metrics.

III. Limitations of Modified Tau

Figure 3 shows the progression of τ_{mod}, t_{pz}, and t_{cpa} during a hypothetical encounter. In this encounter, two aircraft fly at constant velocities with a relative speed of 450 kts (closing) and an HMD of 2000 ft. The

Table 1. Comparison of the three time metrics

Time Metric	Physical Event	Linear with Time	Protecting against Close Intruders
t_{pz}	Yes	Yes	Yes
τ_{mod}	No	No	Yes
t_{cpa}	Yes	Yes	No

D_{mod} corresponding to τ_{mod} and R_0 corresponding to t_{pz} are both set to 4000 ft. No additional buffer zone is allocated for the protected zone corresponding to t_{pz}, i.e., $\Delta_H = 0$. At the beginning of the encounter, τ_{mod} is close to t_{cpa}. The metric τ_{mod} drops more rapidly than time towards t_{pz} as the two aircraft approach the CPA. When $R_0 = D_{\text{mod}}$, Apendix A shows that $t_{pz} \leq \{t_{cpa},\ \tau_{mod}\}$ at any predicted time during the encounter. This is a nice property as any zone defined by a t_{pz} threshold in this condition would enclose the corresponding zone defined by a τ_{mod} or t_{cpa} threshold of the same value.

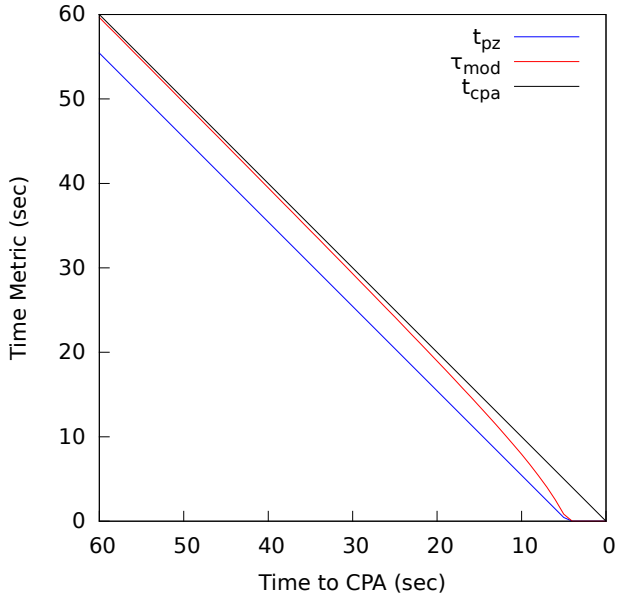

Figure 3. The three time metrics for a head-on encounter.

The Phase I MOPS defines the DWC using a $\tau_{mod} = 35$ sec. An issue with using τ_{mod} for the DWC is that the non-linearity of τ_{mod} adds complexity to an alerting algorithm. For example, very often an alerting algorithm would use the predicted time to a violation of the DWC. Consider a co-altitude, head-on encounter in which two aircraft have zero altitude difference and zero HMD. Suppose the two aircraft's current τ_{mod} is 70 sec, the predicted time for the two aircraft to violate the DWC, however, is not 35 sec into the future. In fact, it must be computed by solving a quadratic equation using $\tau_{mod} = 35$ sec in Eq. 1. Using t_{pz} would avoid this complexity. If the DWC uses a ${t_{pz}}^* = 35$ sec, then current value of 70 sec t_{pz} would mean a predicted loss of DWC 35 seconds into the future.

For alerting, τ_{mod} also has limitations. Since t_{cpa} and t_{pz} correspond to distinct physical events, they can be used directly for prioritizing intruders. The time metric τ_{mod}, on the other hand, cannot be used for this purpose. Figure 4 illustrates a hypothetical encounter involving three non-accelerating intruders with varying relative horizontal speeds and initial values of t_{cpa}. All three intruders have HMD = 0. Here $v \equiv |\dot{\mathbf{r}}|$ denotes the magnitude of an intruder's relative velocity vector. The intruders' initial ranges are $v \times t_{cpa}$. Therefore, intruders (labeled as Intr in the figure) 1, 2, and 3's initial ranges are 1.18, 1.78, and 10.42 nmi, respectively. Without loss of generality, the encounter begins at $t = 0$ sec. Recall that a higher time metric value indicates a lower threat. Intruder 1 (Intr 1) has the smallest relative speed $v = 50$ kts and the largest intial t_{cpa}, $t_{cpa} = 85$ sec. Intruder 1 is predicted by t_{cpa} to be the least threat. On the other hand, τ_{mod} predicts intruder 1 to be the highest threat.

One may argue that the time to the D_{mod} disk serves as a better time metric than t_{cpa} for prioritizing

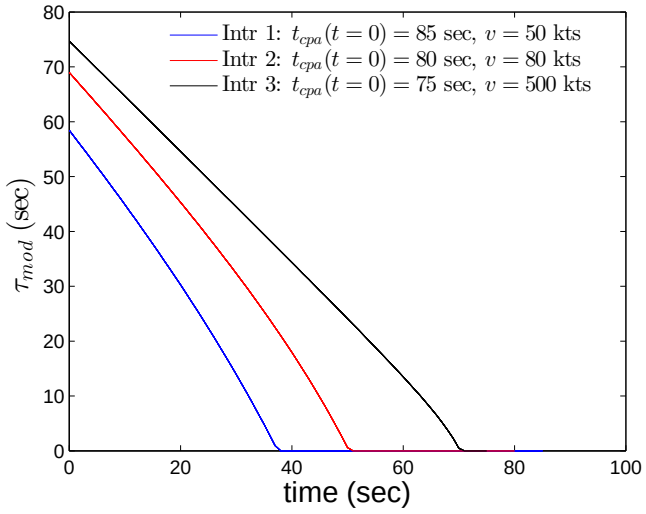

Figure 4. τ_{mod} **ranks intruder threats in reverse order as compared to** t_{cpa} **in a multi-intruder encounter.**

intruders. To test this, consider a protected zone defined by a disk with a radius of D_{mod} with no additional buffer zone. Figure 5 illustrates another hypothetical encounter involving three non-accelerating intruders (different from the previous encounter). All three intruders have HMD = 0. Intruders (labeled as Intr in the figure) 4, 5, and 6's initial ranges are 1.04, 2.67, and 11.81 nmi, respectively. Compared to t_{pz}, τ_{mod} predicts the opposite threat level priorities at the start of the encounter, or time zero. Intruder 4 (Intr 4) has the smallest t_{pz} yet has the largest τ_{mod} 104 sec. Moreover, in this encounter, the intruders' threat level priorities change with time as the τ_{mod} curves intersect. This may be undesirable as it may cause a DAA system's directive guidance to reverse direction during a DAA maneuver.

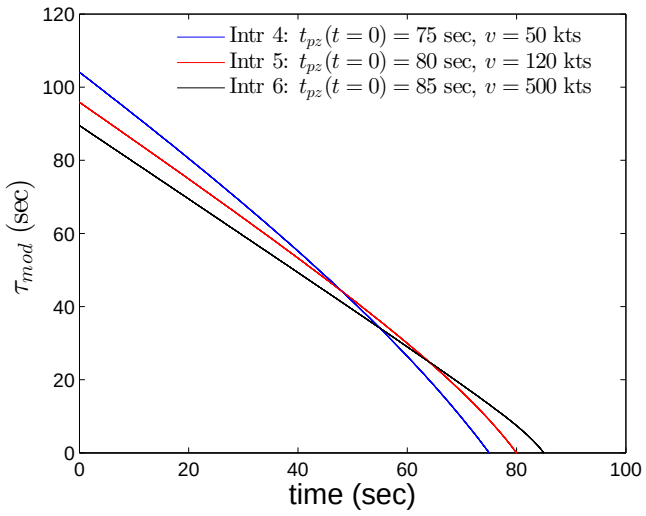

Figure 5. τ_{mod} **ranks intruder threat in reverse order as compared to** t_{pz} **in a multi-intruder encounter.**

IV. Sensitivity to Surveillance Errors

Although t_{pz} has advantages over τ_{mod}, its explicit dependency on aircraft velocities makes it likely to be more sensitive to surveillance errors. Fluctuating values of a time metric around the DAA system's alert threshold are undesirable as it may cause the alert type to vary back and forth, posing challenges in providing a stable, consistent alert display to UAS pilots. Inaccurate values of a time metric may advance or delay the onset of an alert and impact the performance of the DAA system.

Two metrics are defined in this work to measure the sensitivities of t_{pz} and τ_{mod} to surveillance errors:

- Probability of reversal of a time metric during the progression of an non-accelerating encounter, P_r
- Average absolute error of a time metric as a result of surveillance errors, $|\Delta|_{avg}$

Both metrics are equal to zero in the absence of surveillance errors and increase with the magnitude of surveillance errors.

V. Simulations of Encounters

The sensitivities of the time metrics t_{pz} and τ_{mod} to the DAA system's surveillance sensor errors are compared by analyzing a set of simulated encounters with varying geometry, speeds, and surveillance equipage. The metric t_{cpa} is not considered here due to its lack of a protected zone. The DAA simulation system uses true trajectories of the intruder and ownship to compute the true relative trajectories between the aircraft, the simulated surveillance sensor measurements, and the intruder track statistics estimated from the simulated surveillance sensor measurements. The sensor errors are simulated using Honeywell's high fidelity surveillance sensor models and the intruders' tracks are estimated using Honeywell's DAA tracking system. The Honeywell DAA tracker is a sub-TRL6 (Technology readiness level 6) tracker that is in its own iterative development cycle. This is one instantiation of the tracker with expected improvements in later versions to meet the developing DAA requirements and help with better alerting and guidance performance. The data are then collected and used to compute the time metrics and perform subsequent time metric sensitivity analysis. A total of 972 encounters are simulated; the parameters are summarized in the encounter test matrix (see Table 4 in Section VI).

V.A. DAA Simulation System

Figure 6 shows a block diagram of the DAA simulation system. A trajectory generator is used to create the intruder, ownship, and relative intruder trajectories corresponding to the encounters defined in the encounter test matrix. The ownship trajectory is sent to the Ownship Navigation System block where the trajectory is used to provide outputs corresponding to an onboard navigation system. The intruder, ownship, and relative intruder trajectories are sent to the Surveillance Sensor Models block where sensor models are used to simulate ADS-B, Mode-S, Mode-C, and air-to-air radar measurements. The surveillance sensor measurements are sent to the Honeywell Tracking System (HTS). The HTS resolves the surveillance sensor measurements into a common reference frame, uses the H-Fuze system to estimate the track statistics of the intruder relative to the ownship, and computes additional track kinematic statistics required for DAA systems. Finally, the intruder, ownship, and relative intruder trajectories, the ownship navigation solution, and the estimated intruder track statistics are sent to the Time Metric Analysis block for time metric sensitivity analysis.

The HTS is a multi-intruder aircraft, multi-sensor fusion system that estimates the track statistics of intruders relative to the ownship.[12] The HTS fuses the measurements and statistical information from surveillance sensors in one framework to track intruder aircraft in three dimensions. The HTS features the H-Fuze system that performs Data Association, Track Management, and State (or Track) Estimation of surveillance sensors including ADS-B, TCAS, air-to-air radar, optical systems, and ground based radar.

In this encounter trade study, the HTS uses a set of surveillance sensors that includes ADS-B, active surveillance of Mode-S and Mode-C, and air-to-air radar to track intruders. In general, ADS-B sensors provide accurate latitude and longitude measurements and accurate North-South and East-West velocity measurements. Active surveillance sensors provide accurate range measurements, noisy bearing measurements and no velocity measurements. Air-to-air radar provides range measurements with comparable accuracy to active surveillance range measurements and bearing measurements more accurate than active surveillance bearing measurements. Furthermore, air-to-air radar provides North-South and East-West velocity measurements less accurate than ADS-B.

Table 2 summarizes the key surveillance sensor parameters used in the encounter trade studies. Note that these parameters were tuned and verified using flight test data.[18,19] The sensor's fields of view are specified using maximum range (R), bearing (B), and elevation (E). The bearing is defined with respect the line pointed to by the ownship's nose (right is positive). The sensors position errors are specified using latitude, longitude, and altitude for ADS-B; range and bearing for Mode-S and Mode-C; and range, bearing, and elevation for air-to-air radar. The sensor's velocity errors are specified using North (N), East (E), and

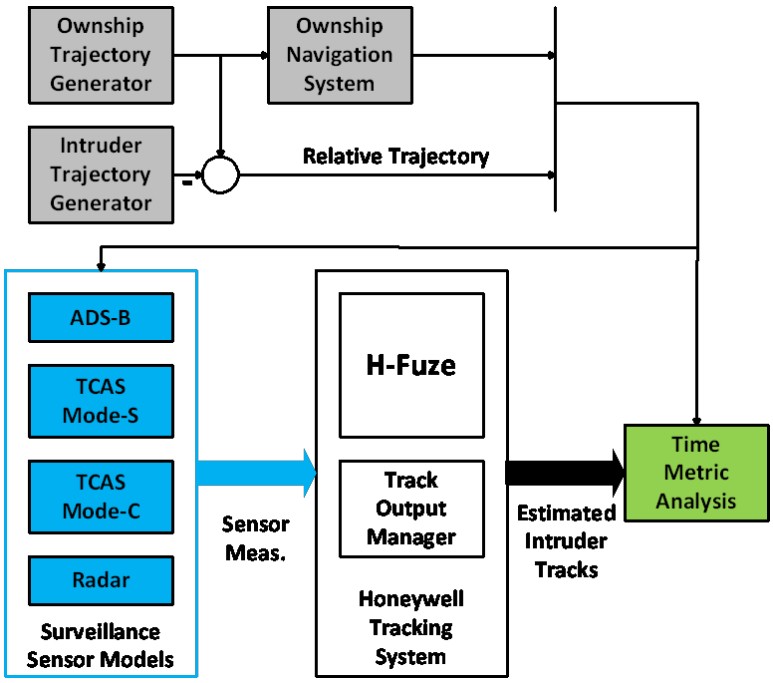

Figure 6. Block diagram illustrating the data flow during the simulation of encounters.

Down (D) for both ADS-B and the air-to-air radar. Mode S and Mode C sensors do not output velocities. Note that the Mode-C range field of view is dependent on the intruders bearing relative to the ownship. Further, note that the Mode-S and Mode-C bearing errors are dependent on the elevation of the intruder relative to the ownship.

Table 2. Key sensor parameters

Type	Field of View [R(nmi), B(deg), E(deg)]	Position Error [lat(deg), lon(deg), alt(m)] or [R(m), B(deg), E(deg)]	Velocity Error [N(m/s), E(m/s), D(m/s)]
ADS-B	[90, 180, 90]	[2, 2, 6.5]	[2, 2, 0.5]
Mode S	[30, 180, 20]	[15 or 9[a] or 5[b], -]	
Mode C	[14[c] 9[d] or 5[e], 180, 20]	[15, 9[f] or 15[g], -]	
Radar	[13, 135, 20]	[10, 0.4, 0.4]	[4, 4, 4]

V.B. Surveillance-Dependent Protected Zone

For DAA alerting criteria, it is desirable to augment the disk-shaped protected zone with a buffer zone. This additional buffer compensates for surveillance errors and reduces fluctuation of alerts. Surveillance errors vary with the sensor type as well as the intruder's relative range and velocity from the ownship. Therefore, the dimensions of the additional buffer zone can potentially be a function of not just the sensor type, but also of other parameters such as the intruder's range, speed, and time to CPA.

[a]when elevation is within $\pm 10°$
[b]when elevation is outside $\pm 10°$
[c]when bearing is within $\pm 45°$
[d]when bearing is between $\pm 45°$ and $\pm 135°$
[e]when bearing is outside $\pm 135°$
[f]when elevation is within $\pm 10°$
[g]when elevation is outside $\pm 10°$

A related consideration is the HMD threshold. For an alerting algorithm that uses an HMD threshold, it seems logical to define an HMD threshold at the edge of the protected zone at $y = 0$. If the protected zone incorporates the HMD in the buffer zone and the HMD threshold is defined appropriately, then the alerting algorithm can provide consistent raw alerts during the progression of an encounter that would lead to a loss of DWC. The choice of the protected zone, as well as the HMD threshold, plays an important factor in a trade-off between missed/late alerts and false alerts.

A conceptually attractive approach is to allow a dynamic protected zone that is a function of the aircraft's estimated tracks as well as surveillance errors. However, in this approach, t_{pz} would no longer be linear with time, and the dimensions of the buffer zone would be a function of encounter geometry and additional sensor parameters. Therefore, estimated tracks are not considered here for defining the protected zone.

This work defines the protected zone such that most of the HMD fluctuations due to surveillance errors during an encounter that would lead to loss of DWC fall within the protected zone. To do so, the HMD error for an intruder is estimated at a characteristic range, R_c, from the ownship, with a characteristic intruder closure rate, v_c. Honeywell sensor model parameters are used for estimating the HMD error. The protected zone is defined by choosing Δ_H to be the estimated HMD error.

For ADS-B, the HMD error arising from range measurement error is independent of range (i.e., a constant error). The HMD error arising from velocity measurement error is proportional to range.

$$\sigma_{H,\ \text{ADS-B}}{}^2 \approx \sigma_{p.\ \text{ADS-B}}{}^2 + \left(\frac{R_c\ \sigma_{v,\ \text{ADS-B}}}{v_c}\right)^2, \tag{5}$$

where $\sigma_{p.\ \text{ADS-B}}$ is the position measurement standand deviation and $\sigma_{v,\ \text{ADS-B}}$ is the velocity measurement standard deviation. For active surveillance, Mode-S or Mode-C,

$$\sigma_{H,\ \text{MODE-S/C}}{}^2 \approx \left(R_c\ \sigma_{b,\ \text{MODE-S/C}}\right)^2, \tag{6}$$

where $\sigma_{b,\ \text{MODE-S/C}}$ is the bearing standard deviation of the Mode-S or Mode-C measurement. For radar,

$$\sigma_{H,\ \text{RADAR}}{}^2 \approx R_c{}^2 * \left(\sigma_{b,\ \text{RADAR}}{}^2 + \frac{\sigma_{v,\ \text{RADAR}}{}^2}{v_c{}^2}\right), \tag{7}$$

where $\sigma_{b,\ \text{RADAR}}$ and $\sigma_{v,\ \text{RADAR}}$ are the bearing and speed standard deviations of the radar measurement, respectively.

The final value of ${\Delta_H}^0$, the superscript denoting a benchmark value, is a function of the combination of sensors,

$$\frac{1}{\left({\Delta_H}^0\right)^2} = \Sigma \frac{1}{\sigma_{H,\ \text{sensor}}{}^2} \tag{8}$$

Table 3 lists the sensor error parameters used for estimating the HMD error and the resulting buffer zone size parameters, ${\Delta_H}^0$. Note that the values in parentheses for ${\Delta_H}^0$ are computed from Eq. 8, and the values before the parentheses are the values actually used in the simulations.

V.C. Encounter Test Matrix

The encounter test matrix for the set of encounters is designed to sample various surveillance equipages, relative speeds, HMDs, relative altitudes, and relative headings. The encounters are intended to cover a wide range of representive parameters but not to model a distribution of encounters.

The methodology for selecting representative intruder equipage types is as follows. The air-to-air radar detects all intruding aircraft as they enter the radar's field of view, subject to the radar's probability of detection. Some intruders are equipped with ADS-B out and are, therefore, detectable by the ownship's ADS-B sensor. The FAA has mandated that, by 2020, all all aircraft operating above 10,000 ft mean sea level (MSL) must be equipped with ADS-B out.[20] Many of the ADS-B out equipped aircraft will also be equipped with a Mode S transponder. Aircraft not equipped with ADS-B may have a Mode S transponder, a Mode C transponder, or no transponder at all. In this work, intruders are categorized by their equipage types in the following way:

- ADS-B out: intruder is detectable by ADS-B and radar.
- Mode S: intruder is detectable by Mode S and radar.

Table 3. Buffer zone parameters and the sensor error parameters used for estimation

Parameter	Value	Unit
R_c	5	nmi
v_c	100	kts
$\sigma_{p,\ \text{ADS-B}}$	2	m
$\sigma_{v,\ \text{ADS-B}}$	2	m/s
$\sigma_{b,\ \text{MODE-S/C}}$	9	deg
$\sigma_{b,\ \text{RADAR}}$	0.4	deg
$\sigma_{v,\ \text{RADAR}}$	4	m/s
$\sigma_{H,\ \text{ADSB}}$	960	ft
$\sigma_{H,\ \text{MODE-S/C}}$	3880	ft
$\sigma_{H,\ \text{RADAR}}$	1930	ft
${\Delta_{H,\ \text{ADS-B}}}^0$	900(860)	ft
${\Delta_{H,\ \text{MODE-S/C}}}^0$	1700(1730)	ft
${\Delta_{H,\ \text{RADAR}}}^0$	1900(1930)	ft

- Mode C: intruder is detectable by Mode C and radar.
- No equipage: intruder is detectable by radar.

Table 4 lists the independent parameters of an encounter defined by the test matrix. The relative speed, altitude, and heading are with respect to the ownship. A relative heading of zero degrees represents a head-on encounter in which the two aircraft are flying towards each other. Passing in front (behind) means the intruder passes in front of (behind) the ownship. The test matrix defines a total of 972 encounters.

Table 4. Parameters of the test matrix

Parameter	Value
Intruder Equipage	ADS-B, Mode S, Mode C, None
Relative Speed (kts)	100, 300, 500
HMD (ft)	0, 1000, 2000, 3000, 4000
Relative Altitude (ft)	-500, 0, 500
Relative Heading (deg)	0, 45, 90
Passing	in front, behind (if HMD$\neq$ 0)

For each encounter, the two time metrics, τ_{mod} and t_{pz}, are computed as follows:

- Kinematics: both the true and estimated ownship navigation solutions and intruder tracks; and
- Protected Zone: using D_{mod} disk and protected zone parameterized by a scaling factor, $\Delta_H/{\Delta_H}^0$, that scales the benchmark HMD error ${\Delta_H}^0$ by 0, 1, 2, and 3. Note that $D_{\text{mod}} = R_0 + \Delta_H$ and $R_0 = 4000$ ft. The reason that D_{mod} is set to $R_0 + \Delta_H$ is because the HMD threshold should be the same as D_{mod} to avoid oscillating alerts.[21]

V.D. Encounter Setup

For each simulated encounter, the ownship is fixed at a specific position and the intruder's initial kinematics are constructed according to the encounter test matrix parameters shown in Table 4, with an initial $t_{cpa} =$ 4 minutes. The intruder trajectories all fly a constant velocity. For analysis of each encounter, both the estimated and true time metrics are computed for tracks with $t_{cpa} < 2$ minutes. The two minute time

window is appropriate for DAA alerts. The time metrics t_{pz} and τ_{mod} are computed for every intruder track estimated by the tracker and the ownship navigation solution with navigation noise. The true time metrics, ${t_{pz}}^0$ and ${\tau_{mod}}^0$, are computed using the true trajectories.

The probability of time reversal, P_r, is calculated from Eq. 9:

$$P_r = \frac{\text{occurrences of increasing time metric in consecutive tracks}}{\text{total number of consecutive tracks}} \tag{9}$$

The average absolute error of a time metric is calculated by averaging the absolute difference between a computed time metric (from the noisy tracks) and its true value (from the true tracks) over the two minute window of the encounter:

$$|\Delta|_{avg} = \frac{\Sigma|t_{pz} - {t_{pz}}^0| \text{ or } \Sigma|\tau_{mod} - {\tau_{mod}}^0|}{\text{total number of tracks}}, \tag{10}$$

where the superscript 0 denotes a time metric computed from the true tracks.

An additional metric, $P(\text{HMD} \leq \text{HMD}^*)$, calculates the percentage of noisy tracks that result in an HMD within the HMD threshold, $\text{HMD}^* = R_0 + \Delta_H$. If the protected zone is wide enough to accommodate HMD errors, this metric should be close to 1.

VI. Simulation Results

Figure 7 shows results aggregated over all encounters of P_r, $|\Delta|_{avg}$, and $P(\text{HMD} \leq \text{HMD}^*)$ at various degrees of extended protected zone, parameterized by the scaling factor $\Delta_H/{\Delta_H}^0$. The general trend is that both P_r and $|\Delta|_{avg}$ decrease as Δ_H increases. The P_r and $|\Delta|_{avg}$ differences between t_{pz} and τ_{mod} are greatest at $\Delta_H/{\Delta_H}^0 = 0$, i.e., no additional buffer zone. Values of P_r are higher for t_{pz} than for τ_{mod} by 14%($\Delta_H/{\Delta_H}^0 = 1$)-50%($\Delta_H/{\Delta_H}^0 = 0$). Values of $|\Delta|_{avg}$ are higher for t_{pz} than for τ_{mod} by 5%($\Delta_H/{\Delta_H}^0 = 1$)-33%($\Delta_H/{\Delta_H}^0 = 0$).

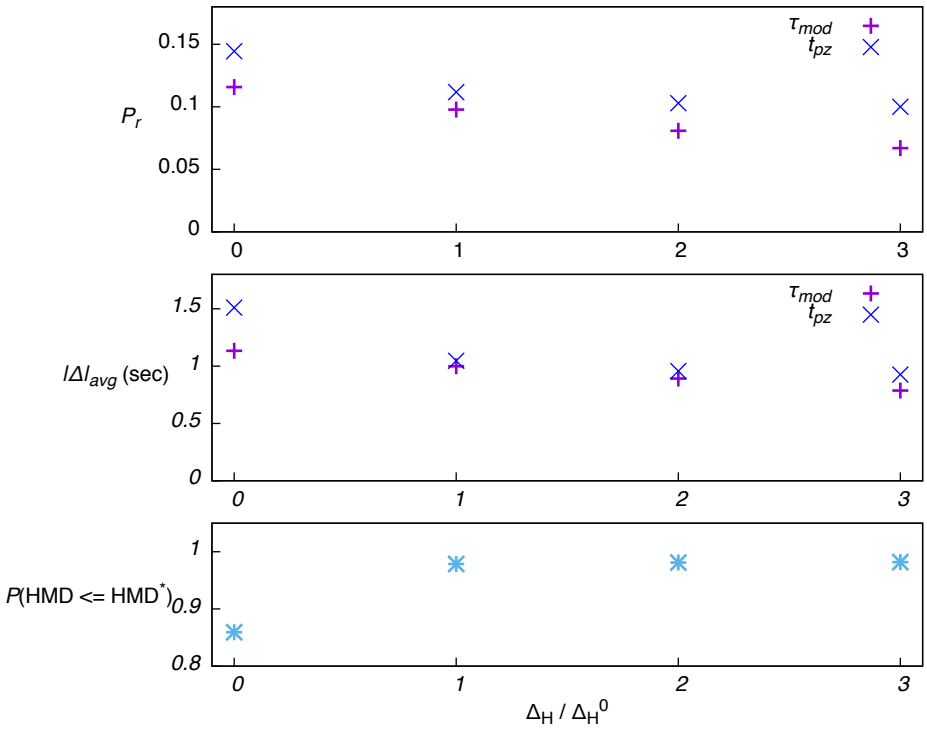

Figure 7. Results of aggregate P_r, $|\Delta|_{avg}$, and $P(\text{HMD} \leq \text{HMD}^*)$.

While the performance of t_{pz} is slightly worse than τ_{mod}, the differences may not be significant enough to degrade the DAA system's alerting performance, especially when $\Delta_H/{\Delta_H}^0 = 1$. In the following paragraphs, only results for $\Delta_H/{\Delta_H}^0 = 1$ are discussed in more detail.

The two sensitivity metrics are highly positively correlated as both increase with the standard deviation of the surveillance errors. Figure 8 shows values of the two metrics for all 972 encounters. The same trends are observed for both metrics in various categories of encounters. Therefore, the following discussion will focus on P_r only.

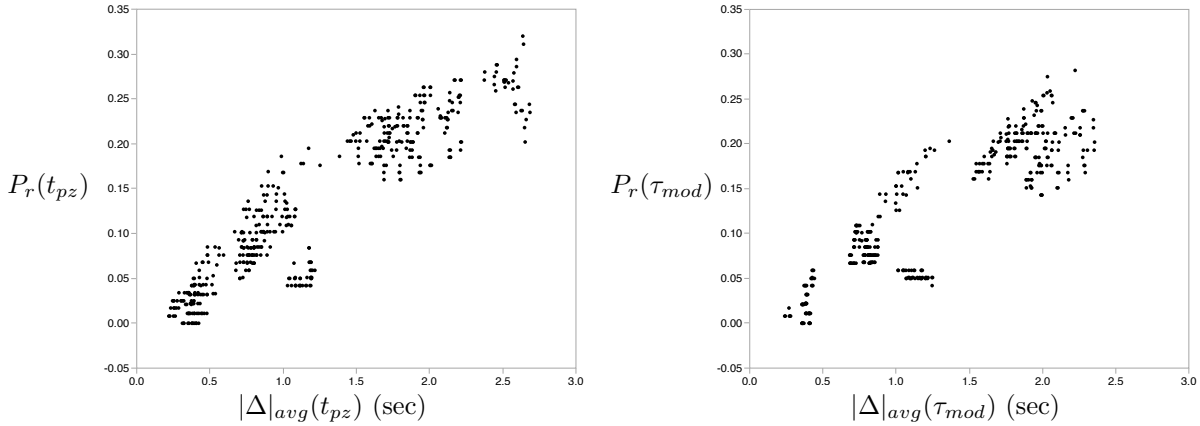

Figure 8. Correlation between P_r (vertical) and $|\Delta|_{avg}$ (horizontal, seconds).

Figure 9 shows the probability of reversal, P_r, categorized by an intruder's relative speed. For both t_{pz} and τ_{mod}, P_r decreases noticeably as the relative speed increases. This trend can be explained as follows. The error of t_{pz} and τ_{mod} can be roughly estimated by

$$\delta t \approx -t\left(\frac{\sigma_r}{r} + \frac{\sigma_{\dot{r}}}{\dot{r}}\right), \tag{11}$$

where σ_r and $\sigma_{\dot{r}}$ represent standard deviations of r and $\dot{r}$, respectively, corresponding to surveillance errors. All four sensors provide very accurate range measurements, and the range error therefore contributes much less than the speed error to the time error. The standard deviation of the speed error in both ADS-B and radar models is not a function of velocity. Therefore, the speed error term on the right side of Eq. 11 is inversely proportional to the magnitude of $\dot{r}$, and therefore is largest when the relative speed itself is small.

A secondary contribution to this trend, although to a lesser extent, is the effect of the sensor's field of view. In high relative speed encounters, the intruder does not enter the sensor's field of view at $t_{cpa} = 120$ seconds but at later times in the encounter. Since the time metric error decreases as the intruder nears the ownship, the later measurement availability lowers the average time metric error.

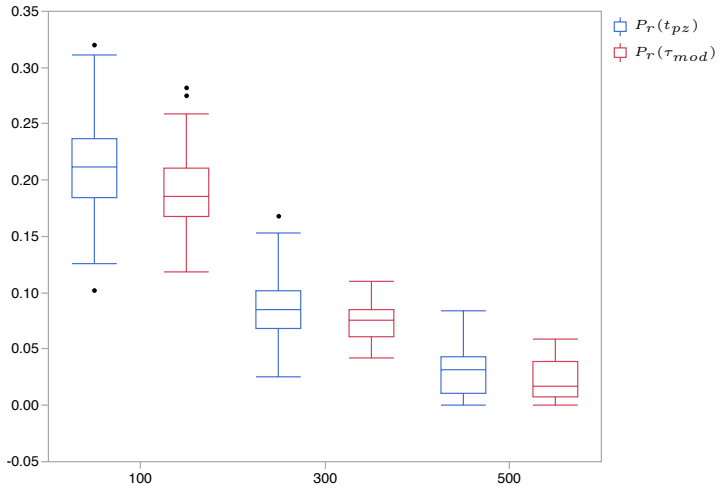

Figure 9. Values of P_r for each relative speed

Comparing t_{pz} results to τ_{mod} results in Figure 9, t_{pz} results in slightly larger median values (the line within the box) at every relative speed.

Figure 10 shows the probability of reversal, P_r, categorized by intruder equipage. Comparing t_{pz} results across categories, intruders with ADS-B out result in the smallest median value of P_r and intruders without any equipage result in the largest median value, approximately 30% greater than the smallest median value. The metric τ_{mod} results display the same trend as the t_{pz} results. Comparing t_{pz} results to τ_{mod} results, t_{pz} leads to a slightly larger median value in every equipage category.

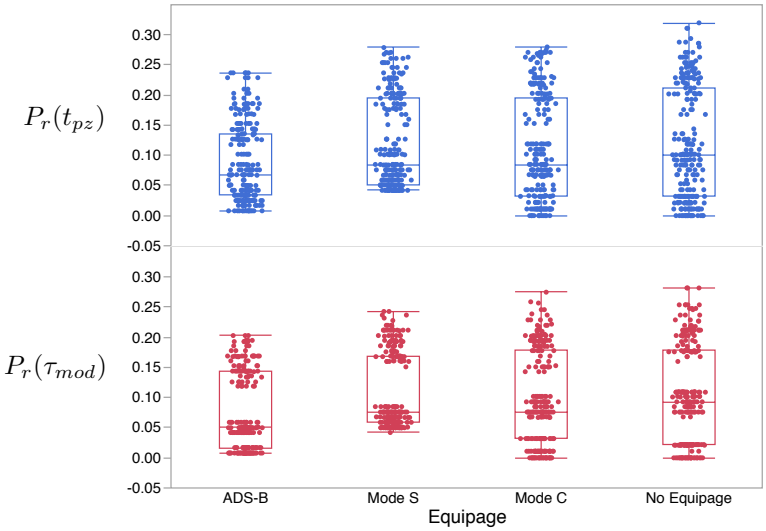

Figure 10. Values of P_r for each intruder equipage category.

Figure 11 shows the probability of reversal categorized by planned HMDs. The probability $P_r(t_{pz})$ increases with HMD, reaching a larger median value and broader distribution at HMD = 4000 ft. This is because the surface of the Protected Zone becomes "steeper" near 4000 ft (see Figure 2) and causes t_{pz} to be more sensitive to HMD errors. On the other hand, P_r distribtions for τ_{mod} are fairly stable across the HMD categories.

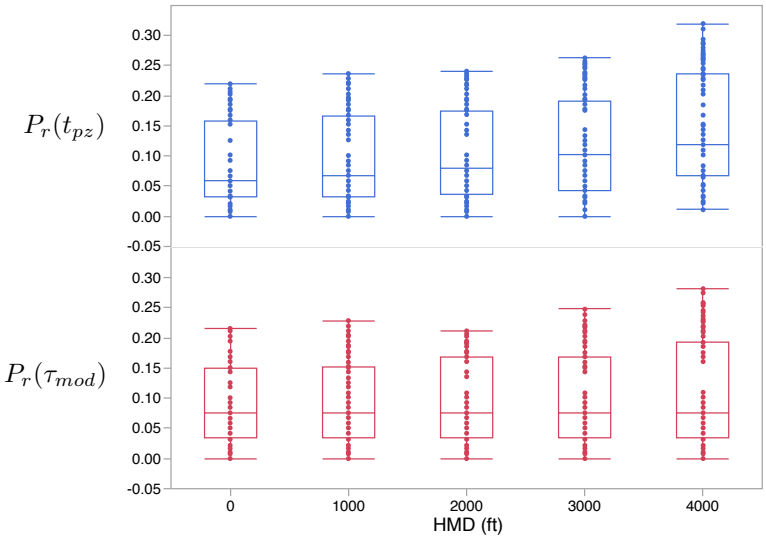

Figure 11. Values of P_r for each value of planned HMD.

The value of P_r shows little variation with relative altitude, relative heading, and the passing direction.

VII. Conclusions

A new time metric called Time to Protected Zone is proposed for use in UAS's Detect and Avoid (DAA) systems. This time metric, denoted as t_{pz}, has three advantages over the currently adopted modified tau, or τ_{mod}. It corresponds to a well-defined physical event, it is linear with the real time during the progression of an encounter, and it can be used directly to prioritize intruders. When used for defining a Well Clear, t_{pz} addresses several limitations of τ_{mod}. For alerting, t_{pz} can be used directly for intruder prioritization while τ_{mod} is limited by its lack of physical interpretation. For alerting, the protected zone can be defined to be a function of surveillance errors for detecting intruding aircraft to provide potentially better alerting performance.

To quantify the sensitivity of t_{pz} to surveillance errors, simulations of encounters using realistic sensor and tracker models are performed. Results show that, with adequately selected protected zones, the sensitivity of t_{pz} to surveillance errors is comparable to that of τ_{mod}. The slight increase of time reversal rates and average time errors by using t_{pz} is likely not enough to impact the alerting performance of a DAA system. Therefore, the choice of t_{pz} over τ_{mod} has advantages and no obvious downside, at least not at a fundamental level. Nonetheless, additional simulations such as MIT Lincoln Lab's encounter models[22] or NASA's NAS-wide simultions[23] that capture a wider variety as well as the statistical nature of encounters must be performed in order to assess the overall performance of t_{pz}.

Appendix: Computation of t_{pz} and Its Relation to τ_{mod}

This section derives the formulas used for computing t_{cpa}, HMD, τ_{mod}, and t_{pz}. The formulas for τ_{mod} and t_{pz} are compared to show that, when $R_0 = D_{\text{mod}}$, $t_{pz} \leq \tau_{mod}$ at all times of the encounter.

Consider an encounter in which an intruder approaches the ownship. By definition,

$$\dot{\mathbf{r}} \equiv \frac{d\mathbf{r}}{dt}. \tag{A.1}$$

The scalar horizontal range r and range rate $\dot{r}$ are defined as

$$\begin{aligned} r &\equiv |\mathbf{r}| \\ \dot{r} &\equiv \tfrac{dr}{dt} = \tfrac{\mathbf{r}\cdot\dot{\mathbf{r}}}{r} \end{aligned} \tag{A.2}$$

For a closing geometry, $\dot{r} < 0$ and $\mathbf{r}\cdot\dot{\mathbf{r}} < 0$. Let $\mathbf{r}$, $\dot{\mathbf{r}}$, r and $\dot{r}$ represent the values at $t = 0$, or the beginning of an encounter. The time metric t_{cpa} is the time at which the predicted r, using constant-velocity trajectories, reaches a minimum. Therefore,

$$(\mathbf{r} + t_{cpa}\dot{\mathbf{r}}) \cdot \dot{\mathbf{r}} = 0, \text{ and} \tag{A.3a}$$

$$t_{cpa} = -\frac{\mathbf{r}\cdot\dot{\mathbf{r}}}{\dot{\mathbf{r}}\cdot\dot{\mathbf{r}}}. \tag{A.3b}$$

If $\dot{\mathbf{r}} \leq \mathbf{0}$, t_{cpa} can be conveniently defined to be 0. The HMD is, by definition, the horizontal distance between the intruder and the ownship at t_{cpa}.

$$\text{HMD} \equiv |\mathbf{r} + t_{cpa}\dot{\mathbf{r}}| \tag{A.4}$$

Taking the square of both sides of Eq. A.4 and substituting Eq. A.3 for t_{cpa}:

$$\text{HMD}^2 = \mathbf{r}\cdot\mathbf{r} - \frac{(\mathbf{r}\cdot\dot{\mathbf{r}})^2}{\dot{\mathbf{r}}\cdot\dot{\mathbf{r}}}. \tag{A.5}$$

Eq. A.5 can be rearranged to derive an expression for $\mathbf{r}\cdot\dot{\mathbf{r}}$, valid when $r \geq \text{HMD}$,

$$\mathbf{r}\cdot\dot{\mathbf{r}} = -|\dot{\mathbf{r}}|\sqrt{r^2 - \text{HMD}^2}, \tag{A.6}$$

where the negative sign indicates a closing geometry.

The time metric t_{pz} is defined as the predicted time for the intruder to reach the protected zone. If the predicted trajectory does not intercept the protected zone, then $t_{pz} = t_{cpa}$. By Eq. (2), it is clear that $t_{pz} \leq t_{cpa}$.

The following paragraphs prove that,

$$t_{pz} \leq \tau_{mod} \text{ when } R_0 = D_{\text{mod}}. \tag{A.7}$$

The additional buffer zone decreases t_{pz} because the resulting protected zone has dimensions larger than the disk of radius R_0. Therefore, it suffices to prove that Eq. A.7 holds when the protected zone is a disk.

When $r \leq D_{\text{mod}}$, both t_{pz} and τ_{mod} are zero and, therefore, Eq. A.7 holds because the intruder is already in the protected zone. When $r > D_{\text{mod}}$, rewrite τ_{mod} as a distance divided by the relative speed, $|\dot{\mathbf{r}}|$:

$$\begin{aligned}
\tau_{mod} &= -\frac{r^2 - {D_{\text{mod}}}^2}{r\dot{r}} \\
&= \frac{1}{|\dot{\mathbf{r}}|}\left[-\frac{r^2 - {D_{\text{mod}}}^2}{\mathbf{r}\cdot(\dot{\mathbf{r}}/|\dot{\mathbf{r}}|)}\right] \\
&= \frac{1}{|\dot{\mathbf{r}}|}\left[\frac{r^2 - {D_{\text{mod}}}^2}{\sqrt{r^2 - \text{HMD}^2}}\right]
\end{aligned} \tag{A.8}$$

where Eqs. A.2 and A.6 are used to derive Eq. A.8. Similarly, rewrite t_{pz} in Eq. 2 as a distance divided by the relative speed, $|\dot{\mathbf{r}}|$, to become

$$\begin{aligned}
t_{pz} &= -\frac{\mathbf{r}\cdot\dot{\mathbf{r}}}{\dot{\mathbf{r}}\cdot\dot{\mathbf{r}}} - \frac{\sqrt{\max\left(0, {D_{\text{mod}}}^2 - \text{HMD}^2\right)}}{|\dot{\mathbf{r}}|} \\
&= \frac{1}{|\dot{\mathbf{r}}|}\left[\sqrt{r^2 - \text{HMD}^2} - \sqrt{\max\left(0,\ {D_{\text{mod}}}^2 - \text{HMD}^2\right)}\right]
\end{aligned} \tag{A.9}$$

Subtracting Eq. A.9 from Eq. A.8 results in

$$\tau_{mod} - t_{pz} = \frac{1}{|\dot{\mathbf{r}}|}\left[-\frac{{D_{\text{mod}}}^2 - \text{HMD}^2}{\sqrt{r^2 - \text{HMD}^2}} + \sqrt{\max\left(0, {D_{\text{mod}}}^2 - \text{HMD}^2\right)}\right]. \tag{A.10}$$

When $\text{HMD} \leq D_{\text{mod}}$,

$$\begin{aligned}
\tau_{mod} - t_{pz} &= \frac{1}{|\dot{\mathbf{r}}|}\left[-\frac{{D_{\text{mod}}}^2 - \text{HMD}^2}{\sqrt{r^2 - \text{HMD}^2}} + \sqrt{{D_{\text{mod}}}^2 - \text{HMD}^2}\right] \\
&\geq \frac{1}{|\dot{\mathbf{r}}|}\left[-\frac{{D_{\text{mod}}}^2 - \text{HMD}^2}{\sqrt{{D_{\text{mod}}}^2 - \text{HMD}^2}} + \sqrt{{D_{\text{mod}}}^2 - \text{HMD}^2}\right] = 0.
\end{aligned} \tag{A.11}$$

When $\text{HMD} > D_{\text{mod}}$, the second term on the right hand side of Eq. A.10 is zero and

$$\tau_{mod} - t_{pz} = \frac{1}{|\dot{\mathbf{r}}|}\left[-\frac{{D_{\text{mod}}}^2 - \text{HMD}^2}{\sqrt{r^2 - \text{HMD}^2}}\right] > 0, \tag{A.12}$$

hence the proof of Eq. A.7 is completed.

References

[1]Cook, S. P., Brooks, D., Cole, R., Hackenberg, D., and Raska, V., "Defining Well Clear for Unmanned Aircraft Systems," *Proceedings of AIAA Infotech@ Aerospace*, AIAA-2015-0481, AIAA, 2015.

[2]Johnson, M., Mueller, E. R., and Santiago, C., "Characteristics of a Well Clear Definition and Alerting Criteria for Encounters between UAS and Manned Aircraft in Class E Airspace," *Eleventh UAS/Europe Air Traffic Management Research and Development Seminar*, 2015, pp. 23–26.

[3]Walker, D., "FAA Position on Building Consensus around the SARP Well-Clear Definition," *RTCA Special Committee*, Vol. 228, 2014.

[4]Murphy, J. R., Hayes, P. S., Kim, S. K., Bridges, W., and Marston, M., "Flight Test Overview for UAS Integration in the NAS Project," *AIAA Atmospheric Flight Mechanics Conference, AIAA SciTech*, AIAA-2016-1756, 2016.

[5]Lee, S. M., Park, C., Thipphavong, D. P., Isaacson, D. R., and Santiago, C., "Evaluating Alerting and Guidance Performance of a UAS Detect-And-Avoid System," NASA/TM-2016-219067, National Aeronautics and Space Administration, Ames Research Center, 2016.

[6]Smearcheck, S., Calhoun, S., Adams, W., Kresge, J., and Kunzi, F., "Analysis of Alerting Performance for Detect and Avoid of Unmanned Aircraft Systems," *IEEE/ION Position, Location and Navigation Symposium (PLANS)*, 2016, pp. 710–730.

[7]Fern, L., Rorie, R. C., Pack, J. S., Shively, R. J., and Draper, M. H., "An Evaluation of Detect and Avoid (DAA) Displays for Unmanned Aircraft Systems: The Effect of Information Level and Display Location on Pilot Performance," *Proceedings of 15th AIAA Aviation Technology, Integration, and Operations Conference*, AIAA-2015-3327, 2015.

[8]Abramson, M., Refai, M., and Santiago, C., "A Generic Resolution Advisor and Conflict Evaluator (GRACE) in Applications to Detect-And-Avoid (DAA) Systems of Unmanned Aircraft," *Proceedings of the 17th AIAA Aviation Technology, Integration, and Operations (ATIO) Conference*, June 2017.

[9]Muñoz, C., Narkawicz, A., Hagen, G., Upchurch, J., Dutle, A., Consiglio, M., and Chamberlain, J., "DAIDALUS: Detect and Avoid Alerting Logic for Unmanned Systems," *34th Digital Avionics Systems Conference (DASC)*, IEEE/AIAA, 2015, pp. 5A1–1.

[10]Suarez, B., Kirk, K., and Theunissen, E., "Development, Integration and Testing of a Stand-Alone CDTI with Conflict Probing Support," *Infotech@ Aerospace 2012*, 2012, p. 2487, Conflict Prediction and Display System (CPDS).

[11]"Introduction to TCAS II Version 7.1," HQ-111358, Federal Aviation Administration (FAA), Feb. 2011.

[12]Bageshwar, V. L. and Euteneuer, E. A., "Multi-Intruder Aircraft, Multi-Sensor Tracking System," *34th Digital Avionics Systems Conference (DASC)*, IEEE/AIAA, 2015, pp. 5A5–1–13.

[13]Muñoz, C., Narkawicz, A., Chamberlain, J., Consiglio, M., and Upchurch, J., "A Family of Well-Clear Boundary Models for the Integration of UAS in the NAS," *Proceedings of the 14th AIAA Aviation Technology, Integration, and Operations (ATIO) Conference*, No. AIAA-2014-2412, Georgia, Atlanta, USA, June 2014.

[14]Narkawicz, A. J., Muñoz, C. A., Upchurch, J. M., Chamberlain, J. P., and Consiglio, M. C., "A Well-Clear Volume Based on Time to Entry Point," NASA/TM-2014-218155, National Aeronautics and Space Administration, Langley Research Center, 2014.

[15]Gazit, R. Y. and Powell, J. D., "Aircraft Collision Avoidance Based on GPS Position Broadcasts," *15th Digital Avionics Systems Conference*, IEEE/AIAA, 1996, pp. 393–399.

[16]Ford, R., "The Protected Volume of Airspace Generated by an Airborne Collision Avoidance System," *Journal of Navigation*, Vol. 39, No. 02, 1986, pp. 139–158.

[17]Upchurch, J. M., Muñoz, C. A., Narkawicz, A. J., Chamberlain, J. P., and Consiglio, M. C., "Analysis of Well-Clear Boundary Models for the Integration of UAS in the NAS," NASA/TM-2014-218280, National Aeronautics and Space Administration, Langley Research Center, 2014.

[18]Gong, C., Wu, M. G., and Santiago, C., "UAS Integration in the NAS Project: Flight Test 3 Data Analysis of JADEM-Autoresolver Detect and Avoid System," NASA/TM-2014-218155, National Aeronautics and Space Administration, Ames Research Center, 2016.

[19]Kotegawa, T., Suarez, B., Gong, C., Bageshwar, V. L., Euteneuer, E. A., Leeper, C., Maki, E., and Theunissen, E., "Proof-of-Concept Airborne Sense and Avoid System with ACAS-X_U Flight Test," *IEEE Aerospace and Electronic Systems Magazine*, Vol. 31, No. 9, 2016, pp. 53–62.

[20]`https://www.faa.gov/nextgen/programs/adsb/faq/#1`.

[21]Muñoz, C. and Narkawicz, A., "Formal Analysis of Extended Well-Clear Boundaries for Unmanned Aircraft," *Proceedings of the 8th NASA Formal Methods Symposium (NFM 2016)*, edited by S. Rayadurgam and O. Tkachuk, Vol. 9690 of *Lecture Notes in Computer Science*, Springer, Minneapolis, MN, June 2016, pp. 221–226.

[22]Weinert, A. J., Harkleroad, E. P., Griffith, J., Edwards, M. W., and Kochenderfer, M. J., "Uncorrelated Encounter Model of the National Airspace System, Version 2.0," Tech. rep., DTIC Document, 2013.

[23]George, S., Satapathy, G., Manikonda, V., Palopo, K., Meyn, L., Lauderdale, T., Downs, M., Refai, M., and Dupee, R., "Build 8 of the Airspace Concept Evaluation System," *AIAA modeling and simulation technologies conference*, 2011, p. 6373.